Expanding the Limits of Laser-Ablation U-Pb Calcite Geochronology

Andrew R.C. Kylander-Clark

Department of Earth Science, University of California, Santa Barbara, CA 93106, USA.

Correspondence to: Andrew R. C. Kylander-Clark (akylander@ucsb.edu)

Abstract. U-Pb geochronology of calcite by laser-ablation inductively-coupled mass spectrometry (LA-ICMPS) is an emerging field with potential to solve a vast array of geologic problems. Because of low levels of U and Pb, measurement by more sensitive instruments, such as those with multiple collectors (MC), is advantageous. However, whereas measurement of traditional geochronometers (e.g., zircon) by MC-ICPMS has been limited by detection of the daughter isotope, U-Pb dating of calcite can be limited by detection of the parent isotope, if measured on a Faraday detector. The *Nu P3D* MC-ICPMS employs a new detector array to measure all isotopes of interest on Daly detectors. A new method, described herein, utilizes the low detection limit and high dynamic range of the *Nu P3D* for calcite U-Pb geochronology, and compares it with traditional methods. Data from natural samples indicates that measurement of ^{238}U by Daly is advantageous at count rates <30,000; this includes samples low in U or those necessitating smaller spots. Age precision for samples run in this mode are limited by ^{207}Pb counts and the maximum U/Pb$_c$. To explore these limits—i.e., the minimum U, Pb, and U/Pb ratios that can be measured by LA-ICPMS—a model is created and discussed; these models are meant to serve as a guide to evaluate potential candidate materials for geochronology. As an example, for samples necessitating a <1 Ma uncertainty, a minimum of ~10 ppb U is needed at a spot size of 100 µm and rep rate of 10 Hz; absolute uncertainty scales roughly with U concentration.

1. Introduction

Calcite U-Pb geochronology by laser-ablation inductively-coupled mass spectrometry (LA-ICPMS) is a relatively new technique with untapped potential for solving numerous geochronologic problems from the timing of faulting (e.g., Roberts and Walker, 2016; Nuriel et al., 2017; Goodfellow et al., 2017), age of ore deposits (Burisch et al., 2017) to paleoclimate, sedimentation, and diagenesis (e.g., Mangenot et al., 2018; Rasbury et al., 1997; Hoff et al., 1995; Winter and Johnson, 1995; Wang et al., 1998; Rasbury et al., 1998). Early studies focused on carbonates more likely to contain high concentrations of U, such as speleothems (e.g., Richards et al., 1998) because the method employed—thermal ionization mass spectrometry (TIMS)—required weeks to produce reliable ratios; samples with a low likelihood of success, that is, those with potentially low U contents, were ignored. With the advent of LA-ICPMS, however, sample throughput and analytical costs have been greatly reduced, such that hundreds of geoanalytical facilities can, at the very least, screen a large number of samples and choose those suitable for geochronology in a relatively short period of time and for little cost; sample preparation is minimal, several samples can be analyzed in a day, and dozens of labs worldwide have the capability to perform such analyses. LA-ICPMS also has the advantage of sampling smaller volumes of material; it can thus take advantage of the heterogenous nature of calcite with respect to U and Pb, using larger datasets to better constrain both the initial $^{207}Pb/^{206}Pb$ compositions and the common Pb-corrected concordia ages. These isochron ages are calculated with ease on a Tera-Wasserburg diagram similar to other common-Pb-bearing mineral chronometers like titanite and apatite (e.g., Chew et al., 2014; Spencer et al., 2013), but calcite also lends itself to a ^{208}Pb-based correction, given that it usually contains low levels of Th (Parrish et al., 2018).

For typical LA-ICPMS analyses, a 193 nm excimer laser is employed in conjunction with either a single-collector (SC-ICPMS; either a quadrupole or sector-field instrument), or multi-collector (MC-ICPMS) sector-field instrument. Traditionally, an MC-ICPMS uses a series of Faraday detectors on the high-mass side of the detector array to measure ^{238}U and ^{232}Th, and either Faraday cups or secondary electron multipliers (SEMs) on the low-mass side of the array to concurrently measure Pb isotopes; SC-ICMPS instruments measure isotope count rates sequentially with a single SEM. The SC and MC instruments have distinct advantages. Because there is only one SEM on a SC-ICPMS instruments, there is no need to cross calibrate multiple detectors, yielding simpler data reduction and the possibility for making 204- or 208-based common-Pb corrections (e.g., Parrish et al., 2018). An MC-ICPMS, on the other hand, is 2–3 times more sensitive than the top SC-ICPMS instruments. This allows precise measurements of samples with low levels of Pb (i.e., young and/or low common-Pb). Furthermore, its *equivalent* sensitivity is even higher because it measures all masses at the same time. For example, a SC-ICPMS running only masses 238, 207, and 206 (232, 208, and 204 are also typically measured) at equal dwell times measures 1/3 the counts over a given cycle than the count rate might suggest because only one mass can be measured at a time; given that it is also 2-3x less sensitive than an MC-ICPMS, a laser spot must be ~6-9 times bigger to achieve the same precision on a SC-ICPMS. However, expected count rates for each isotope are different, and a SC-ICPMS can be configured to count longer on lower-concentration elements, thus reducing the precision offset between the two instruments. A further advantage of an MC-ICPMS is that transient signals from changes in U and Pb concentration during ablation affect uncertainties in the measured $^{207}Pb/^{206}Pb$ and $^{206}Pb/^{238}U$ less because all measurements are made concurrently; similarly, it also eliminates transient signals due to ICP flicker. Finally, the smaller dynamic range of the SEM can limit samples to a specific range of U concentrations; samples or reference materials with high U contents can cause the detector to trip to a different measurement mode (or trip off), yielding spurious results. Low U concentrations in calcite can also be a problem for an MC-ICPMS measuring ^{238}U with a Faraday cup because limits of detection are on the order of 10^4 cps. Conversely, a SC-ICPMS can precisely measure count rates of ~10^2 cps by employing a secondary electron multiplier (SEM) for all masses. However, because of an SC-ICPMS is 2-3 times less sensitive, the range of low-U samples that can only be measured by SC-ICPMS is rather limited.

Fortunately, a recently introduced MC-ICPMS—the *P3D*—by *Nu Instruments* (Wrexham, UK) can overcome both of these limitations. The instrument features a Daly detector array that allows for ion counting on ^{238}U and the Pb isotopes, and thus expands the range of calcite samples—those with lower U concentrations—that can be precisely measured by LA-ICPMS. Similar to a standard SEM, the Daly detector allows for increased sensitivity over a faraday cup, but it does so with a greater dynamic range (approx. 10-fold over that of an SEM) and with a more linear response. Thus equipped, the instrument can effectively analyze samples with a larger range of U concentrations; from 10^2–10^7 cps. This contribution describes the analytical setup for LA-ICPMS using the new *Nu P3D*, comparing the two modes with each other and with that of a SC-ICPMS, and thereby demonstrating the increased capability of this new instrumentation to measure calcite U-Pb dates. Further, by presenting data from three different instrument setups, and by comparing these results to those expected from theoretical models, the aim of this contribution is also to serve as a guide for those interested in U-Pb calcite geochronology.

2 Experimental Setup

The analytical setup is described in Table 1. The instrumentation used in the study consists of a *Photon Machines Excite* 193 nm excimer laser equipped with a HelEx cell, coupled to a *Nu Instruments P3D* for standard LA-ICPMS analyses. The *Nu Plasma 3D* (*P3D*) contains an array with 6 Daly detectors, 5 on the low-mass side of the array and 1 on the high-mass side. A 14-Faraday array lies between the Daly detectors, and allows for measurement of ^{238}U on either a Faraday or Daly detector, depending on the U concentration in the sample. Daly detectors are used to measure masses 202, 204, 206, 207, and 208, and ^{232}Th is measured on a Faraday cup. Faraday backgrounds yield a 1SD of 0.04 mV, which implies a limit of detection (LOD) of ~0.1 mV or ~8000 cps; Daly backgrounds yield 1SD of 10–20 cps for isotopes of Hg and Pb and 1 cps for ^{238}U, corresponding to LODs of 30–60 and 3 cps, respectively.

In order to compare the difference between SC and MC analytical sensitivities and uncertainties, the laser was used in conjunction with the *P3D* for two experiments, and an *Agilent 7700* Q-ICPMS for one experiment. These 3 experiments were run with different spot sizes: *Experiment F*) a 65 µm spot on the *P3D* using a Faraday for masses 238 and 232, and Daly detectors for masses 208–204 and 202 (110 total analyses); *Experiment D*) the same configuration, but with 238 measured on a Daly detector; and *Experiment Q*) a 110 µm spot with the Q-ICPMS and cycle times of 0.06, 0.13, 0.1, and 0.1 s on masses 238, 207, 206, and 204 respectively. During each separate analytical run, each spot was located near the corresponding spot from the other runs, to minimize uncertainty caused by grain homogeneity. For all experiments, the laser was run at 10 Hz for 15 seconds and a fluence of approximately 1 J/cm^2, yielding a spot depth of 10–15 µm. Analyses were preceded by two pre-ablation pulses, and 20 seconds of baseline measurement.

Three calcite samples—veins associated with faulting—from the Champlain Valley of western Vermont (courtesy of W. Amidon of Middlebury College) were the main samples measured. These samples—C258, C304, and C273—are ca. 440, 110, and 80 Ma, respectively, and range in U concentration between a few ppb and a few ppm, with an average of 120 ppb and a mode of ~20 ppb. Three further samples (C254, C283A, and C283B), were run in experiments F and D and provide more data for uncertainty comparisons between the two instrumental configurations (see Figure 1), but the data are described in less detail; they are ca. 440 Ma with variable Cretaceous (?) (re)crystallization. Calcite and NIST614 reference materials (RMs) were interspersed every 10 analyses, and a two-stage reduction scheme was employed. *Iolite v.3.0* (Paton et al., 2011) was used first used to correct the $^{207}Pb/^{206}Pb$ for mass bias, detector efficiency, instrumental drift etc., and to correct the $^{238}U/^{206}Pb$ ratio for instrumental drift, using NIST614 as the primary reference material. During this first data reduction, 2 seconds were removed from both the beginning and end of both the RMs and the unknowns, yielding a total count time of 11 s. The $^{238}U/^{206}Pb$ ratio was then corrected using a linear correction in *Excel* such that the primary calcite RM, WC-1, yielded 254 Ma (Roberts et al., 2017) on a Tera-Wasserburg (TW) diagram, anchored to a $^{207}Pb/^{206}Pb$ value of 0.85. Similar to that of the $^{207}Pb/^{206}Pb$ ratio, this correction encompasses offset due to both mass bias and detector efficiency differences (i.e., there is no prior gain calibration for the Daly detector array). Using this method, we retrieved ages of 3.01 ± 0.15 (MSWD = 1.3; n = 30) and 65.9 ± 1.1 (MSWD = 1.2; n = 40) for secondary RMs ASH15 (2.96 Ma; Nuriel et al., 2020) and Duff Brown Tank (64 Ma; Hill et al., 2016), respectively. Because the purpose of this study is to gain a better understanding of the analytical equipment uncertainties associated with the standards (e.g., upper intercept of WC-1, $^{207}Pb/^{206}Pb$ value of NIST614, etc.) were not propagated into the uncertainties of unknown analyses. Analyses with large uncertainties (arbitrarily chosen as 50% for both $^{238}U/^{206}Pb$ and $^{207}Pb/^{206}Pb$) were discarded; removing these data has little influence on the final age. The data from the unknowns are all a bit scattered for geological reasons, and were culled to yield single populations for ease of comparison (Though beyond the scope of this manuscript, the Paleozoic samples are interpreted to have suffered partial Pb loss or new crystal growth in the Cretaceous–Tertiary, and the older Cretaceous sample likely (re)crystallized over an extended period.)

3 Results

Table 2 and Figure 2 shows the results for the 6 samples analyzed in the 3 experiments. *Experiment F (P3D – 65 µm spot; U on a Faraday)* yielded ~170 kcps/ppm (2.7 mV/ppm) of mass 238 on NIST614 and was relatively stable throughout the run. The sensitivity of *Experiment D (P3D – 65 µm spot; U on a Daly)* was similar to that of *Experiment F*, but dropped approximately 25% during the analytical session to ~125 kcps/ppm (2 mV/ppm) of mass 238 on NIST614. *Experiment Q (Agilent Q-ICPMS – 110 µm spot)* yielded ~110 kcps/ppm of mass 238 on NIST614—equivalent to ~1.8 mV/ppm from a spot ~3 times larger than the 65 µm spot in experiments 1 and 2—and was stable throughout the run.

For every sample, Experiment F yielded fewer analyses with uncertainties of <50% for $^{206}Pb/^{238}U$, as well as the fewest spots available to make an isochron; this is depicted graphically in Figure 1b as a steeper negative slope for Experiment F vs Experiments D and Q. These results are consistent with a higher average and median U ppb (Table 2); low U concentrations that were measured in Experiments D and Q went undetected or yielded large uncertainties in Experiment F. Though samples with median ^{238}U count rates of >10,000 cps (C273C and C304A) returned fewer viable analyses and worse average $^{238}U/^{206}Pb$ uncertainties in Experiment F, the uncertainty of the final age was similar for the higher-U samples on both configurations on the *P3D*; both yielded lower uncertainties than the Q-ICPMS, despite the 3-fold volume increase in analyzed material on the Q-ICPMS (Figure 2).

When average count rates of ^{238}U were below ~8000 cps (near the detection limit of the Faraday detector on the *P3D)*, however, the number of viable analyses and final age precision was significantly higher in

Experiment D (Table 2 and Figure 2). As an example, sample C258 yielded few viable data points (35% of the 110 analyses) in Experiment F, fewer than half the number of good analyses in Experiments D and Q. In addition, the resulting uncertainty in the final age calculation (~4%) is significantly larger than that of Experiment D, and similar to the resulting uncertainty in Experiment Q (although the Q-ICPMS yielded >2 times the number of viable spots). Samples C283A and C283C—which also contain low levels of U—yielded ~50% fewer viable data, necessitated double the average count rates of ^{238}U, and final uncertainties that were significantly greater in Experiment F than those of Experiment D.

A summary of the precision vs. U count rate is shown in Figure 1, which shows the precision of $^{238}U/^{206}Pb$ and ^{238}U on a single spot vs. the count rate of ^{238}U. While there is considerable overlap in the precision vs. ^{238}U cps of both ^{238}U and $^{238}U/^{206}Pb$ at count rates above approx. 30,000 cps, data collected in Experiment F yielded no better than a few kcps 2σ uncertainty on ^{238}U (Fig. 1a); $^{238}U/^{206}Pb$ uncertainties consequently show a similar deviation from the high-count-rate trend (Fig. 1b). Finally, though the Q-ICPMS shows similar gains in precision for low-U analyses, the lower sensitivity of the Q-ICPMS results in a smaller window of U concentrations for which analyses have lower uncertainties than those run on the *P3D* (vertical offset in symbols in Fig. 1b).

4 Discussion

While there is a clear advantage of using the new Daly-only detector setup on the *P3D* for LA-based calcite geochronology for some samples, the extent to which this advantage obtains for all samples is still somewhat ambiguous. The samples that benefit most from the new instrumentation are not only low in U, but also older. For most measurements of long-lived-isotope geochronology, the analytical limit is determined by the detection limit of the daughter, not the parent, isotope. However, because older samples have more daughter product, they are—for samples with low U/Pb_c ratios—more likely to be limited by the count rate of the parent isotope. For samples run on a SC-ICPMS, this distinction is unimportant because the detection limit of ^{238}U is in all cases lower than that for Pb. However, because the MC-ICPMS has a large sensitivity and precision advantage over the SC-ICPMS, it is important to distinguish the limits of measurement between the Faraday–Daly and all-Daly configuration.

4.1 Theoretical uncertainty of Tera–Wasserburg data

To explore the limits of precision for each analytical configuration, a synthetic dataset was created (using an *MS Excel* spreadsheet; available on request) to represent different U/Pb_c and ^{238}U cps for samples of different ages. Figure 3 shows samples with ages of 440, 80, and 15 Ma with error ellipses at U/Pb_c ratios of 1, 2, 5, 10, 20, 100 and 200. The size of the ellipse is the maximum possible uncertainty (from counting statistics only) for a 10s analysis, given the limit of detection of the instrument. For the all-Daly configuration, the limit of detection is determined by ^{207}Pb counts, the least abundant isotope of interest. For this example, 30 cps is assumed (the best achieved LODs herein; Hansman et al., 2018), but it is important to recognize that the LOD of Pb is based on the background, which varies from lab to lab, and is also a function of the instrumental sensitivity. For the Faraday–Daly arrangement, the LOD is limited by ^{238}U counts for samples with lower U/Pb_c and by ^{207}Pb for samples with high U/Pb_c—and increasingly so as the sample age decreases. In this case, a minimum of 30,000 cps of ^{238}U is considered—as opposed to the actual ca. 8000 cps LOD—for the Faraday, because that is the count rate below which a distinct benefit in precision is gained by using the all-Daly arrangement (see Figure 1 and discussion above). As depicted in Figure 3, older samples yield the greatest range of U/Pb_c ratios that could yield an advantage of measurement by ^{238}U on an ion counter, whereas the advantage of the Daly detector disappears at U/Pb_c ratios greater than ca. 500 and 250 for samples that are 80 and 15 Ma, respectively. As an example of the benefit of ^{238}U measurement by Daly, an 80 Ma sample with a maximum U/Pb_c ratio of 10 yields 1400 cps of ^{238}U at the LOD of 30 cps ^{207}Pb. Given a limit of detection of 8000 cps for the Faraday detector, the signal size would need to be 6 times higher before it could be measured by such means. Furthermore, as discussed above, and shown in Figure 1, the benefit of the Daly extends to ca. 30,000 cps, or ~20 times the signal that can be measured by the Faraday–Daly configuration. The benefit extends to 200 times for a U/Pb_c ratio of 1; but some question arises as to the ability to measure ages at such low U/Pb_c values.

4.2 Choosing Samples and Instruments

One intention of this manuscript is to serve as a guide to determine whether any given calcite (or any other Pb_c-bearing) sample is appropriate for U–Pb geochronology, and deciding which type of analytical equipment to use. As such, the model above is expanded below to explore the U/Pb_c ratios and count rates needed to produce a reliable age from a given number of analyses. These models are then compared with the natural results to determine best practices when selecting samples and instruments for analysis.

4.2.1 U and Pb_c distribution in calcite

Calculating theoretical limits is complicated, however, because the uncertainty of an isochron depends on the distribution of U, Pb_c, and thus the distribution of U/Pb and Pb/Pb ratios. For example, a sample with a given maximum U/Pb_c will yield a final precision that increases with the number of analyses, but this improvement depends on the distribution of the U/Pb_c ratios. The distribution of U and Pb, and thus $^{238}U/^{206}Pb$ and $^{207}Pb/^{206}Pb$, in calcite has not been a particular subject of study (but see Roberts et al., 2020), but a cursory analysis of the reference materials and unknowns presented in this manuscript shows that U and Pb concentrations follow normal distributions; RMs that contain sufficient U (WC-1 and Duff Brown Tank) display a near- normal distribution of U, whereas the distribution of U concentration of samples and RMs with lower U contents (ASH15 and unknowns) are log normal (Figure 4). Like U, Hg-corrected ^{204}Pb counts (a proxy for common Pb) are normally distributed in RMs and unknowns; ^{208}Pb counts are similar. The resulting $^{238}U/^{206}Pb$ ratios of RMs are normally distributed, but unknowns vary and can be rather uniform (e.g., C273C). The manner by which the type of distribution affects the final uncertainty is demonstrated in Figure 5. The precision of a T-W isochron is best defined by precisely defined end points with maximum spread; as such, except for samples with extreme U/Pb_c, a uniform distribution of $^{238}U/^{206}Pb$ ratios results in better final age precision than does a normal distribution. For example, a sample that is 440 Ma with normally distributed data (and ratios $\pm 3\sigma$ from the mean) requires nearly 2 times as many points to achieve the same precision as a sample with uniformly distributed data over the same U/Pb range (Figure 5d; though this also depends on the maximum U/Pb_c). For normally distributed data with the same maximum U/Pb_c, but only 50% of the spread (i.e., more tightly clustered; Figure 5b), the number of necessary data points increases further, excepting samples with extreme U/Pb_c (these data would be less dependent on the precision of the upper intercept).

4.2.2 U and Pb_c distribution in calcite

To compare theoretical data with that obtained from this study—i.e., in order to best represent a natural dataset—we present and discuss models (using the same *Excel* sheet as that in Section 4.1) with 100 uniformly distributed $^{238}U/^{206}Pb$ data points acquired for 10 s at 10 Hz, recognizing that, as stated above, this is likely a best-case scenario. We explore the implications of varying maximum U/Pb_c ratios rather than $^{238}U/^{206}Pb$ ratios because the former are independent of sample age. The results of the model are shown in Figure 6. Because the precision of analyses in an ion-counter-only configuration is limited by the count rate of ^{207}Pb, we calculate the maximum U/Pb_c ratio that can be achieved for different concentrations of U. For example, a 440 Ma sample with 10 ppb U run with a 65 µm spot size will yield ~1500–2000 cps of U (star symbol in Figures 6a, 6b, 6c). The maximum U/Pb_c that could be achieved with this count rate will be ~13, because any higher values will yield too few counts of ^{207}Pb to be measured. Assuming constant U concentration and normally distributed $^{238}U/^{206}Pb$ ratios, the best precision on the age of this sample is 0.6%—considerably better than expected for LA-ICPMS (e.g., Horstwood et al., 2016). As a comparison, sample C283A contains an average of 10 ppb U (and maximum of 40 ppb) and thus yields a similar average count rate of ^{238}U. Its maximum U/Pb_c of 26 is considerably less than the maximum theoretical value based on the concentration of that particular analysis because its Pb concentration is well above detection. It should be no surprise then, that the age uncertainty is higher than the theoretical value at that count rate, but it is also higher than the theoretical value for a U/Pb_c of 26. Several factors may explain this: 1) though 100 analyses were measured, 32 were imprecise and rejected; 2) the distribution of $^{238}U/^{206}Pb$ ratios is not uniform; 3) laser instability, detector response time, laser-induced elemental fractionation (LIEF), signal instability, etc. add uncertainty beyond that based on counting statistics; and 4) low U/Pb$_c$ values likely have less U and Pb than in the model.

Although optimistic, this model serves as a guide for the limitation of analyses of calcite by LA-ICPMS, given U concentration, maximum U/Pb$_c$, and spot size. First, for all but the youngest samples (<<15 Ma), measurement with the *P3D* can be advantageous for samples with lower U or those necessitating small spot sizes (e.g., <150 ppb U and <70 µm, or <50 ppb U and <125 µm; symbols in Figure 6a); this is shown as the light- and dark grey areas in Figure 6 (i.e., the area below the “no Daly benefit line” in Figure 6e). However, if, for example, the sample contains concentrations >100 ppb U and the spot can be >100 µm, there is no advantage to using the all-Daly configuration, and if there is significant material (i.e., spot size can be >200 µm), any LA-ICPMS will provide the best possible results (that is, the precision will be limited not by the count rate, but rather other factors such as differences in LIEF, matrix effects etc.). Second, it is highly unlikely that even with extreme spot sizes and rep rates, that samples with <<1 ppb U can be analyzed. Third, older samples—when run on the *P3D*—reach their best possible uncertainty (ca. 2%) with U concentrations of 10–15 ppb; samples as young as 80 Ma require little more than 30 ppb U, and samples as young as 15 Ma require up to 150 ppb U at moderate spot sizes. Though 2% final uncertainty requires greater concentrations of U for younger samples (>2500 cps ^{238}U are needed for an 80 Ma sample, and >12,000 cps ^{238}U for a 15 Ma sample), it should be noted that—at a given concentration, spot size and U/Pb$_c$—absolute uncertainty is relatively independent of age; for example, a sample with a 65 µm spot and 10 ppb U yields an uncertainty of just over 2 Ma, whether the sample is 15, 80, or 440 Ma. Finally, though not depicted directly in Figure 6, precise ages can be obtained from data with rather low U/Pb$_c$ values. For example, 100 spots with 2% uncertainty yields a final uncertainty of 5–15 Ma (2σ) for samples with U/Pb$_c$ ratios as low as 1–2. That said, data with such low U/Pb$_c$ ratios should be viewed with caution, as systematic uncertainties—such as those introduced by inconsistencies in RM isotopic measurements—can lead to large errors when extrapolating data clustered near the upper intercept.

4.3 More spots, deeper spots, or bigger spots?

The theoretical models discussed above use a 10 sec integration time to compare the models to the empirical data. As discussed above, precision can be improved by increasing the number of analytical spots, but each spot can also be ablated for longer or at a higher rep rate (i.e., making deeper pits rather than more pits). One might imagine that these methods might be equally effective, however, there are two important points to consider. First, individual spot precision is limited to the long-term reproducibility of down-hole measurements, and is generally no better than 2%; this precision is more difficult to assess in calcite because most known reference materials exhibit moderate isotopic heterogeneity (e.g., Roberts et al., 2017). Thus, if increasing the depth of the pit yields analytical uncertainties <2%, then the excess pit depth is wasted and overall uncertainty fails to improve. Second, whereas increasing the number of spots leads to a linear increase in the total number of counts (and thus an increase in precision by $\sqrt{n}$), an increase in pit depth does not lead to a linear increase in counts because ablation yields decrease with pit depth. Thus, if an increase in total counts could yield better precision, that increase should come from more, shallower laser pits, rather than fewer, deeper pits.

It is also possible to increase precision by increasing the spot size. In fact, an argument could be made that a SC-ICPMS that measures 250 µm spots is just as effective as a MC-ICPMS that measures 100 µm spots. Though this argument has merit, the downside is twofold; 1) some regions of interest are simply not large enough to permit a spot 2.5X as wide, and 2) U and/or Pb (i.e., U/Pb_c) may be heterogeneous at scales smaller than the spot size, mixing calcite of different age or reducing the range of isotopic ratios that are used to construct an isochron. Figure 7 demonstrates that even though larger spots can yield a better per-spot precision, analyzing the same volume of material with smaller spots can yield better age precision because it can take advantage of the heterogeneous U and Pb concentrations typical of calcite.

5 Conclusions

1) Unlike geochronometers with high U and little to no common Pb—such as zircon and monazite—U-Pb dates of minerals with low U and significant common Pb can be limited by the count rates of the parent U, rather than the daughter Pb.

2) Given a limit of detection of ~8000 cps for on a Faraday, and the sensitivity of the *Nu P3D*, samples with as low as 20 ppb U can be analyzed with a 100 µm spot at 10 Hz, and as low as 5 ppb for a 200 µm spot. Even so, the Faraday is less precise than the Daly at count rates of <30,000 cps, corresponding to U concentrations of ca. 75 and 20 ppb, with the same respective spot sizes and rep rates.

3) When ^{238}U is analyzed on a Daly, the limit of detection drops by a factor of >1000, and the analytical capability is thus limited by the LOD of Pb—^{207}Pb in almost all cases—and the ratio required for optimum precision. The typical LOD of ^{206}Pb and ^{207}Pb is ca. 50 cps; it is greater for higher sensitivity instruments, and those with a higher background of common Pb. For a desired U/Pb_c ratio of ca. 5–10 for old and young samples, respectively, the required count rate of ^{238}U would be 500–1000 cps or ca. 5–10 times smaller than can be analyzed on a Faraday detector. The analysis of ^{238}U on a Daly, therefore increases the analytical capability to ca. 0.5–2 ppb U for a 100–200 µm spot, respectively.

4) Although the % uncertainty that can be achieved with limited concentrations of U is considerably different among samples with different ages, the absolute uncertainty is approximately the same. For example, samples with 1500 cps ^{238}U yield a maximum possible uncertainty of ca. 2 Ma, nearly independent of age (older samples yield slightly higher absolute uncertainties). However, because most LA-ICPMS facilities can achieve up to 2% precision on final age calculations, younger samples can yield better absolute uncertainties; these can only be achieved at high U concentrations, which limits the advantage of the *Nu P3D* for young samples.

5) Given enough material and analytical time, a SC-ICPMS, should, in theory, be capable of measuring samples with concentrations of approximately 2–10 times (i.e., 1–20 ppb U) that of the *Nu P3D*.

However, because of their lower cycle times and inability to make concurrent measurements, SC-ICPMS instruments likely require considerably higher concentrations of U to obtain comparable date precision.

Code Availability

The code described in this manuscript is available on request from the author

Data Availability

All data described herein is contained within the data supplement

Sample Availability

These samples were limited to 1 in. epoxy mounts. If necessary, the author can inquire with the provider should one like access to the sample(s).

Competing Interests

The author declares that he has no conflicts of interest.

Acknowledgements

This paper was greatly improved by the reviews of D. Chew and R. Parrish.

Figure Captions

Figure 1. Relation between cps ^{238}U and uncertainty of ^{238}U (A), and $^{206}Pb/^{238}U$ (B). Grey lines in A are %2SE uncertainties of ^{238}U. The 3 experiments show the same trend in uncertainty vs. cps at count rates above ~30 kcps 238, but below that, uncertainty of measurements in Experiment F (238 on the Faraday) increase significantly compared to Experiments D and Q. Although Experiments D and Q (red and blue symbols) show the similar trends, the sensitivity gain using the P3D leads to significant improvements in spot uncertainty; large symbols represent expected uncertainties for a 100 um spot at 10 ppb U and the vertical offset between them represents the gain or loss in precision for such an analyses depending on instrumentation used.

Figure 2. Tera–Wasserburg concordia diagrams of the 3 unknown samples in each of the 3 experiments. See text for discussion.

Figure 3. Uncertainty ellipses for each Tera–Wasserburg plot depict two end-member type of analyses in which the large ellipses represent the limit of detection of the all-Daly configuration, or any SC-ICPMS (limited by ^{207}Pb counts), and the smaller ellipses represent the uncertainty at 30,000 cps ^{238}U, the point at which measurement of ^{238}U on the Daly is no advantageous. The ellipses are colored according to the ^{238}U count rate, and depict the counting uncertainty for a 10 s analysis at the given count rate and different U/Pb$_c$ ratios of 1, 2, 5, 10, 20, 50, 100, 200. Example analyses are illustrated in each of the panels at different U/Pb$_c$ ratios of 5 (440 Ma; 3A), 20 (80 Ma; 3C), and 50 (15 Ma; 3B).

Figure 4. Left-hand plots show the difference in distribution of ^{238}U/^{206}Pb ratios in reference materials and unknowns; ratios are nomalized to the ^{238}U/^{206}Pb ratio of the age of the sample. Reference materials Duff Brown and WC-1 have the smallest variation in ^{238}U/^{206}Pb ratios, which correlates well with the distribution of their U and Pb contents (left-hand plots). Reference material ASH15 and unknown sample C283C still have a wider log-normal distribution, reflective of their larger distribution of U and Pb contents relative to Duff Brown and WC-1. Unknown sample C273C has a more uniform distribution of ^{238}U/^{206}Pb ratios, reflecting its largest distribution of U contents.

Figure 5. A-C shows an example of the differing randomly generated distributions of 100 analyses with the same maximum U/Pb$_c$. 5A shows a normal distribution for the entire range of U/Pb$_c$; 5B is a normal distribution over the upper 50% of the same range. The uniform distribution, shown in 5C, yields the lowest uncertainties because there are more analyses at both the upper and lower intercepts. D shows how the percent uncertainty decreases with number of analyses, depending on the type of ^{238}U/^{206}Pb distribution depicted in A–C; data in D assumed the best case scenario of 2% uncertainty per data point and a U/Pb$_c$ ratio of 10 for samples of 440 Ma, 80 Ma, and 15 Ma. Best uncertainties are achieved with uniform distributions and maximum spread. Although percent uncertainties are always better for older samples, younger samples yield better absolute uncertainties for well distributed data.

Figure 6. 6A shows the count rate expected with the Nu P3D given for a given spot size at a laser energy of ~1 J/cm2 and 10 Hz. 6B, D, F show the maximum U/Pb_c that can be achieved with the given U concentration and spot size (colored contours); the star symbol in 6B illustrates an example that a 65 µm spot with 10 ppb U can yield a U/Pb_c no better than ~13, otherwise ^{207}Pb will be below detection (i.e., <30 cps; example explained in text). Colored circles indicate analyses of unknowns in Experiment F (^{238}U on the Faraday; Table 2; 65 µm, average U ppb); color represents the maximum U/Pb_c ratio—taken from Table 2—and the size represents the final uncertainty. Note that the maximum U/Pb_c correlates with U concentration. In all plots, the grey area (dark and light) represents the region in which measurement of ^{238}U on a Daly is advantageous to that on a Faraday; open and filled diamonds in 6A represent examples in text in which spots smaller or lower in U are favorably measured on the Daly detector. Dark grey region represents spot sizes and U concentrations too low for measurement on a Faraday detector. 6C, E, and G show the best possible uncertainty (colored contours) at the given count rates and spot sizes for 100 analyses, all with the same U concentration but a uniform distribution of ^{238}U/^{206}Pb ratios. Star symbol in 6C explained in text.

Figure 7. Tera–Wasserburg diagram representing the analysis of a heterogeneous medium using different spot sizes. Though the bigger spot sizes yield smaller individual uncertainties, the smaller spots take advantage of the spread in U/Pb_c ratios and thus yield a better overall uncertainty on the lower intercept age.

References

Burisch, M., Gerdes, A., Walter, B. F., Neumann, U., Fettel, M., and Markl, G.: Methane and the origin of five-element veins: Mineralogy, age, fluid inclusion chemistry and ore forming processes in the Odenwald, SW Germany, Ore Geology Reviews, 81, 42-61, 10.1016/j.oregeorev.2016.10.033, 2017.

Chew, D. M., Petrus, J. A., and Kamber, B. S.: U-Pb LA-ICPMS dating using accessory mineral standards with variable common Pb, Chemical Geology, 363, 185-199, 10.1016/j.chemgeo.2013.11.006, 2014.

Goodfellow, B. W., Viola, G., Bingen, B., Nuriel, P., and Kylander-Clark, A. R.: Palaeocene faulting in SE Sweden from U-Pb dating of slickenfibre calcite, Terra Nova, 29, 321-328, 2017.

Hill, C. A., Polyak, V. J., Asmerom, Y., and P. Provencio, P. C. T. C.: Constraints on a Late Cretaceous uplift, denudation, and incision of the Grand Canyon region, southwestern Colorado Plateau, USA, from U-Pb dating of lacustrine limestone, Tectonics, 35, 896-906, 10.1002/2016tc004166, 2016.

Hoff, J. A., Jameson, J., and Hanson, G. N.: Application of Pb Isotopes to the Absolute Timing of Regional Exposure Events in Carbonate Rocks - an Example from U-Rich Dolostones from the Wahoo Formation (Pennsylvanian), Prudhoe Bay, Alaska, Journal of Sedimentary Research Section a-Sedimentary Petrology and Processes, 65, 225-233, 1995.

Horstwood, M. S. A., Košler, J., Gehrels, G., Jackson, S. E., McLean, N. M., Paton, C., Pearson, N. J., Sircombe, K., Sylvester, P., Vermeesch, P., Bowring, J. F., Condon, D. J., and Schoene, B.: Community-Derived Standards for LA-ICP-MS U-(Th-)Pb Geochronology – Uncertainty Propagation, Age Interpretation and Data Reporting, Geostandards and Geoanalytical Research, 10.1111/j.1751-908X.2016.00379.x, 2016.

Mangenot, X., Gasparrini, M., Gerdes, A., Bonifacie, M., and Rouchon, V.: An emerging thermochronometer for carbonate-bearing rocks: Delta(47)/(U-Pb), Geology, 46, 1067-1070, 10.1130/G45196.1, 2018.

Nuriel, P., Weinberger, R., Kylander-Clark, A. R., Hacker, B., and Craddock, J.: The onset of the Dead Sea transform based on calcite age-strain analyses, Geology, 45, 587-590, 2017.

Nuriel, P., Wotzlaw, J.-F., Stremtan, C., Vaks, A., and Kylander-Clark, A. R.: The use of ASH15 flowstone as matrix-matched standard for laser-ablation geochronology of calcite, Geochronology, 2, https://doi.org/10.5194/gchron-2020-22.

Parrish, R. R., Parrish, C. M., and Lasalle, S.: Vein calcite dating reveals Pyrenean orogen as cause of Paleogene deformation in southern England, Journal of the Geological Society, 175, 425-442, 10.1144/jgs2017-107, 2018.

Paton, C., Hellstrom, J., Paul, B., Woodhead, J., and Hergt, J.: Iolite: Freeware for the visualisation and processing of mass spectrometric data, Journal of Analytical Atomic Spectrometry, 26, 2508-2518, 10.1039/c1ja10172b, 2011.

Rasbury, E. T., Hanson, G. N., Meyers, W. J., and Saller, A. H.: Dating of the time of sedimentation using U-Pb ages for paleosol calcite, Geochimica Et Cosmochimica Acta, 61, 1525-1529, Doi 10.1016/S0016-7037(97)00043-4, 1997.

Rasbury, E. T., Hanson, G. N., Meyers, W. J., Holt, W. E., Goldstein, R. H., and Saller, A. H.: U-Pb dates of paleosols: Constraints on late Paleozoic cycle durations and boundary ages, Geology, 26, 403-406, Doi 10.1130/0091-7613(1998)026<0403:Updopc>2.3.Co;2, 1998.

Richards, D. A., Bottrell, S. H., Cliff, R. A., Strohle, K., and Rowe, P. J.: U-Pb dating of a speleothem of Quaternary age, Geochimica Et Cosmochimica Acta, 62, 3683-3688, Doi 10.1016/S0016-7037(98)00256-7, 1998.

Roberts, N. M. W., and Walker, R. J.: U-Pb geochronology of calcite-mineralized faults: Absolute timing of rift-related fault events on the northeast Atlantic margin, Geology, 44, 531-534, 10.1130/G37868.1, 2016.

Roberts, N. M. W., Rasbury, E. T., Parrish, R. R., Smith, C. J., Horstwood, M. S. A., and Condon, D. J.: A calcite reference material for LA-ICP-MS U-Pb geochronology, Geochemistry Geophysics Geosystems, 18, 2807-2814, 10.1002/2016GC006784, 2017.

Spencer, K. J., Hacker, B. R., Kylander-Clark, A. R. C., Andersen, T. B., Cottle, J. M., Stearns, M. A., Poletti, J. E., and Seward, G. G. E.: Campaign-style titanite U-Pb dating by laser-ablation ICP: Implications for crustal flow, phase transformations and titanite closure, Chemical Geology, 341, 84-101, 10.1016/j.chemgeo.2012.11.012, 2013.

Wang, Z. S., Rasbury, E. T., Hanson, G. N., and Meyers, W. J.: Using the U-Pb system of calcretes to date the time of sedimentation of elastic sedimentary rocks, Geochimica Et Cosmochimica Acta, 62, 2823-2835, Doi 10.1016/S0016-7037(98)00201-4, 1998.

Winter, B. L., and Johnson, C. M.: U-Pb Dating of a Carbonate Subaerial Exposure Event, Earth and Planetary Science Letters, 131, 177-187, Doi 10.1016/0012-821x(95)00026-9, 1995.

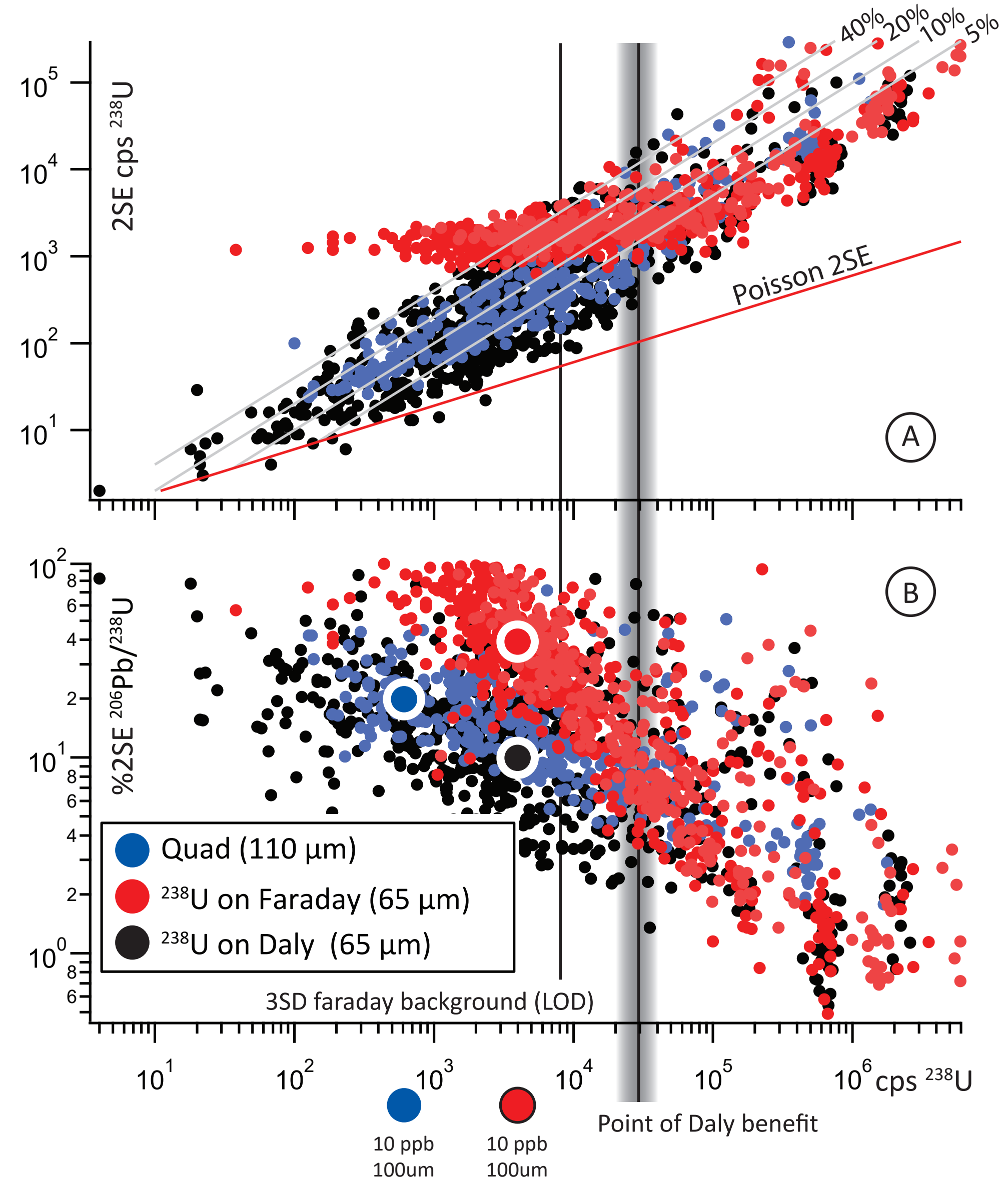

Figure 1. Relation between cps 238U and uncertainty of 238U (A), and 206Pb/ 238U (B). The 3 experiments show the same trend in uncertainty vs. cps at count rates above ~30 kcps 238, but below that, uncertainty of measurements in Experiment F (238 on the Faraday) increase significantly compared to Experiments D and Q. Although Experiments D and Q (red and blue symbols) show the similar trends, the sensitivity gain using the P3D leads to significant improvements in spot uncertainty (large symbols represent expected uncertainties for a 100 um spot at 10 ppb U).

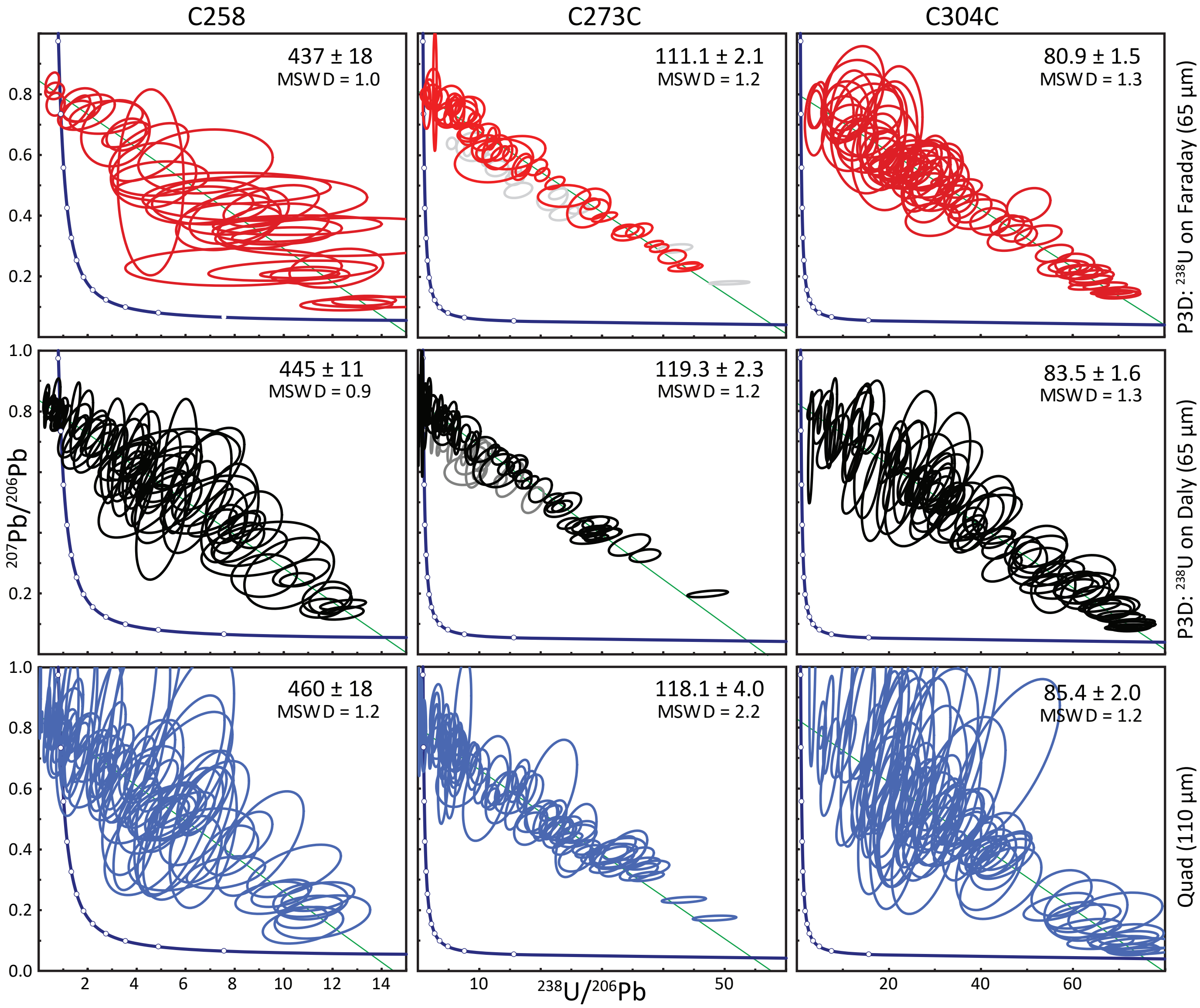

Figure 2. Tera–Wasserburg concordia diagrams of the 3 unknown samples in each of the 3 experiments. See text for discussion.

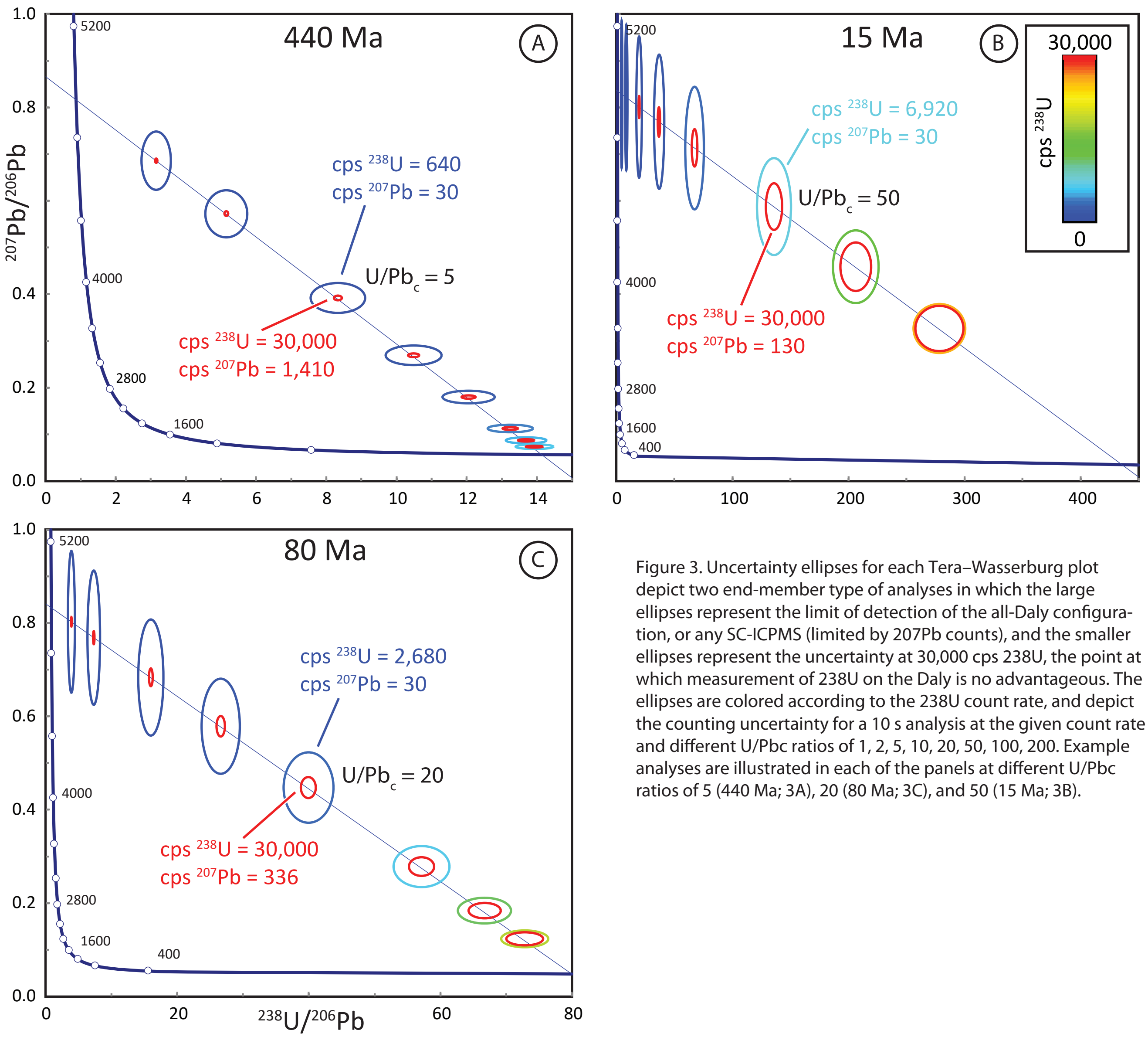

Figure 3. Uncertainty ellipses for each Tera–Wasserburg plot depict two end-member type of analyses in which the large ellipses represent the limit of detection of the all-Daly configuration, or any SC-ICPMS (limited by 207Pb counts), and the smaller ellipses represent the uncertainty at 30,000 cps 238U, the point at which measurement of 238U on the Daly is no advantageous. The ellipses are colored according to the 238U count rate, and depict the counting uncertainty for a 10 s analysis at the given count rate and different U/Pbc ratios of 1, 2, 5, 10, 20, 50, 100, 200. Example analyses are illustrated in each of the panels at different U/Pbc ratios of 5 (440 Ma; 3A), 20 (80 Ma; 3C), and 50 (15 Ma; 3B).

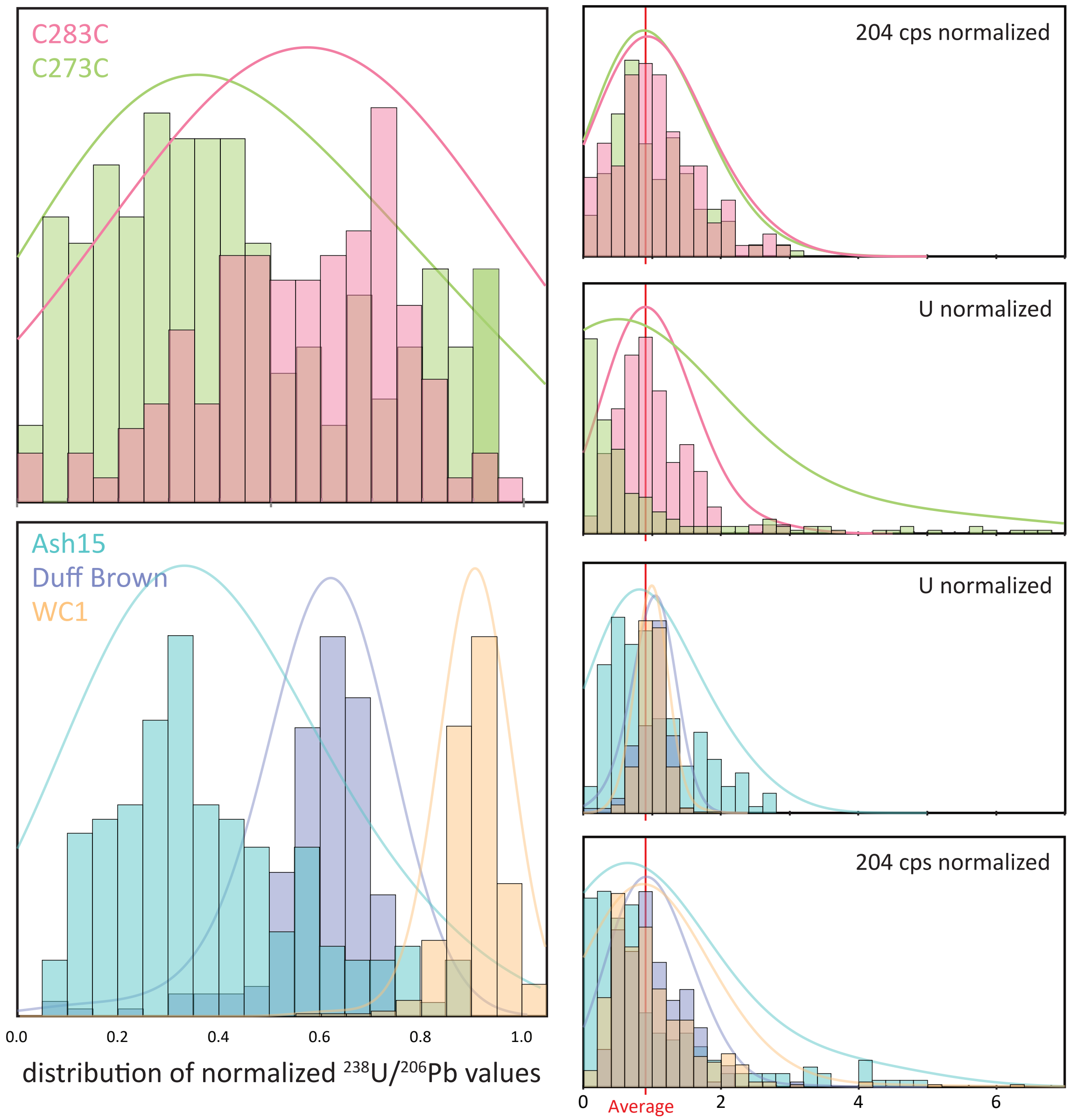

Figure 4. Left-hand plots show the difference in distribution of 238U/206Pb ratios in reference materials and unknowns; ratios are nomalized to the 238U/206Pb ratio of the age of the sample. Reference materials Duff Brown and WC-1 have the smallest variation in 238U/206Pb ratios, which correlates well with the distribution of their U and Pb contents (left-hand plots). Reference material ASH15 and unknown sample C283C still have a wider log-normal distribution, reflective of their larger distribution of U and Pb contents relative to Duff Brown and WC-1. Unknown sample C273C has a more uniform distribution of 238U/206Pb ratios, reflecting its largest distribution of U contents.

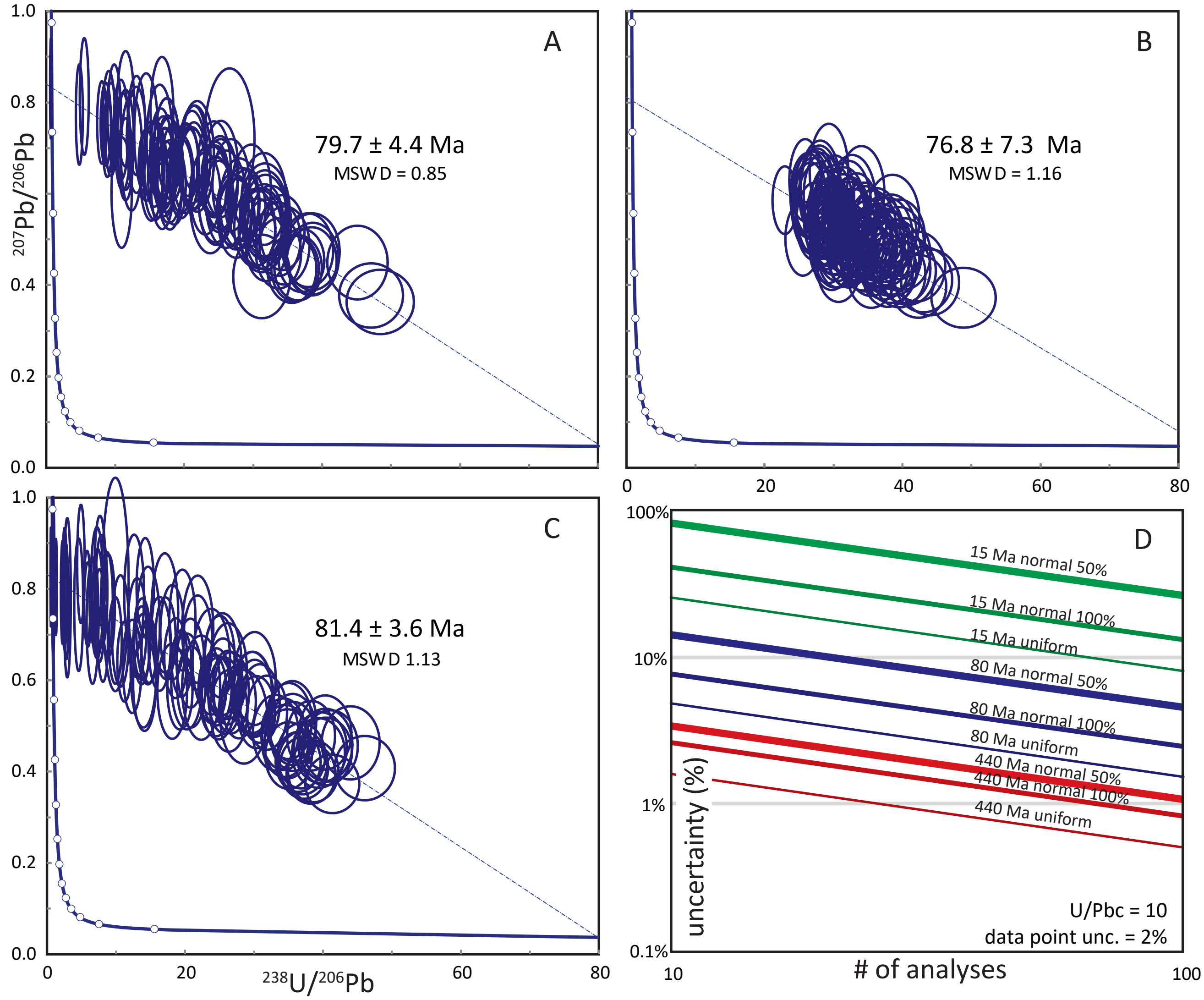

Figure 5. A-C shows an example of the differing randomly generated distributions of 100 analyses with the same maximum U/Pbc. 5A shows a normal distribution for the entire range of U/Pbc; 5B is a normal distribution over the upper 50% of the same range. The uniform distribution, shown in 5C, yields the lowest uncertainties because there are more analyses at both the upper and lower intercepts. D shows how the percent uncertainty decreases with number of analyses, depending on the type of 238U/206Pb distribution depicted in A–C; data in D assumed the best case scenario of 2% uncertainty per data point and a U/Pbc ratio of 10 for samples of 440 Ma, 80 Ma, and 15 Ma. Best uncertainties are achieved with uniform distributions and maximum spread. Although percent uncertainties are always better for older samples, younger samples yield better absolute uncertainties for well distributed data.

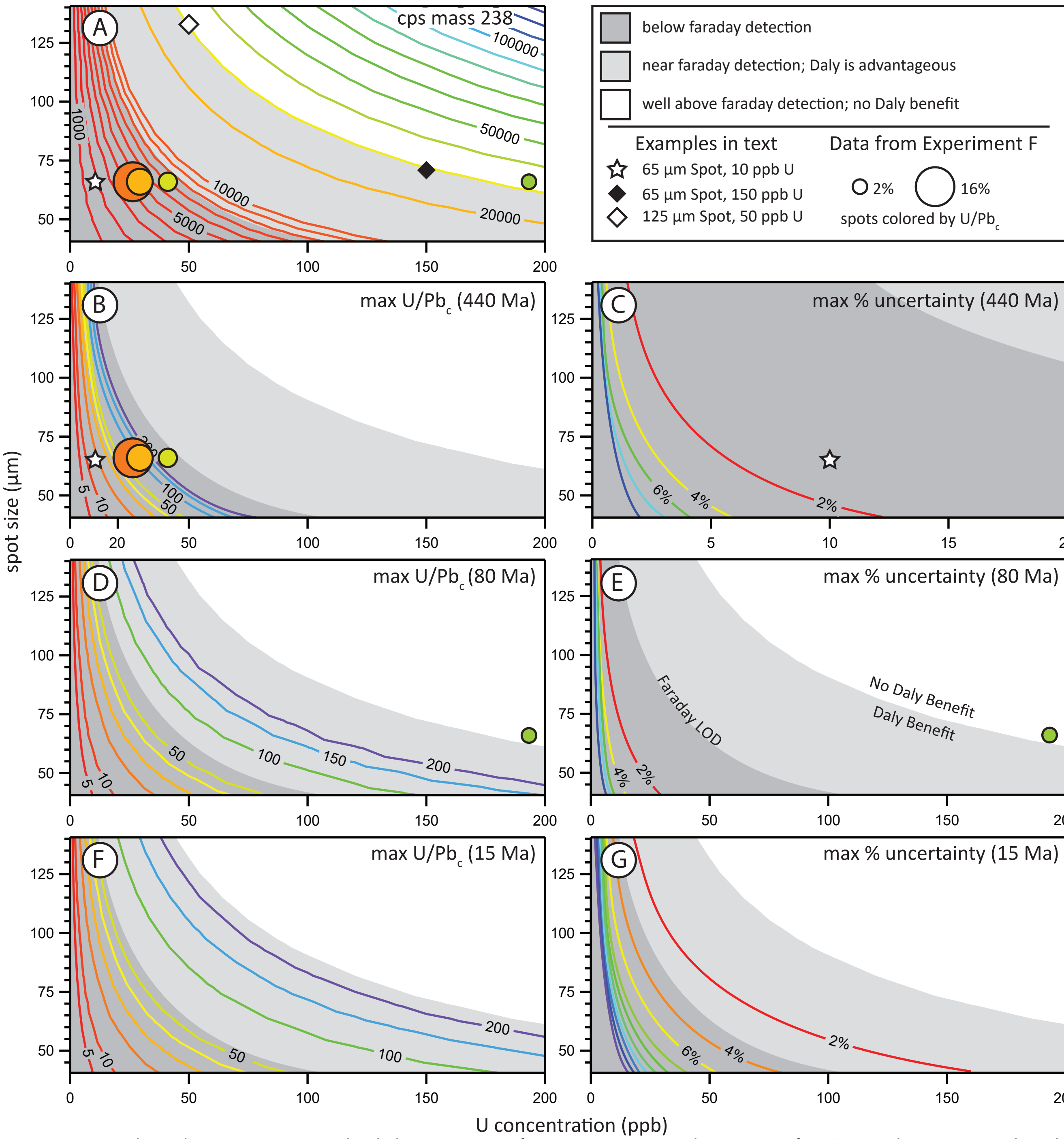

Figure 6. 6A shows the count rate expected with the Nu P3D given for a given spot size at a laser energy of ~1 J/cm2 and 10 Hz. 6B, D, F show the maximum U/Pbc that can be achieved with the given U concentration and spot size (colored contours); the star symbol in 6B illustrates an example that a 65 µm spot with 10 ppb U can yield a U/Pbc no better than ~13, otherwise 207Pb will be below detection (i.e., <30 cps; example explained in text). Colored circles indicate analyses of unknowns in Experiment F (238U on the Faraday; Table 2; 65 µm, average U ppb); color represents the maximum U/Pbc ratio—taken from Table 2—and the size represents the final uncertainty. Note that the maximum U/Pbc correlates with U concentration. In all plots, the grey area (dark and light) represents the region in which measurement of 238U on a Daly is advantageous to that on a Faraday; open and filled diamonds in 6A represent examples in text in which spots smaller or lower in U are favorably measured on the Daly detector. Dark grey region represents spot sizes and U concentrations too low for measurement on a Faraday detector. 6C, E, and G show the best possible uncertainty (colored contours) at the given count rates and spot sizes for 100 analyses, all with the same U concentration but a uniform distribution of 238U/206Pb ratios. Star symbol in 6C explained in text.

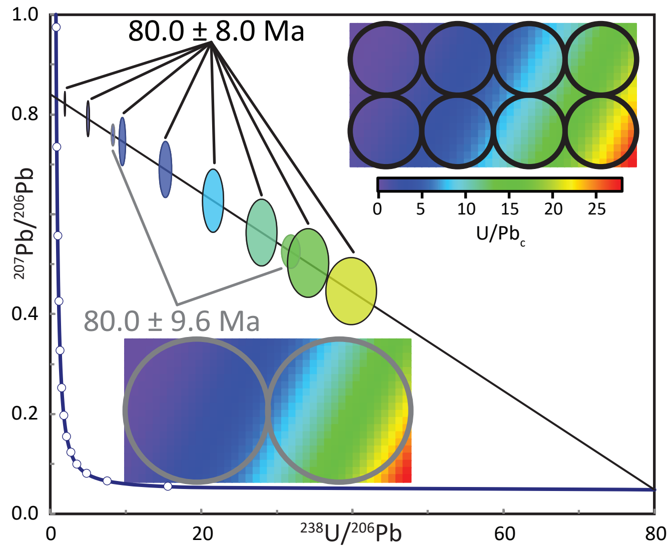

Figure 7. Tera–Wasserburg diagram representing the analysis of a heterogeneous medium using different spot sizes. Though the bigger spot sizes yield smaller individual uncertainties, the smaller spots take advantage of the spread in U/Pbc ratios and thus yield a better overall uncertainty on the lower intercept age.

Table 1.
Instrumental parameters of laser-ablation split-stream ICP-MS

	MC-ICP-MS	Q-ICP-MS
Instrument model	Nu Plasma 3D	Agilent 7700x
RF forward power	1300 W	1300 W
RF reflected power	<10 W	<10 W
Coolant gas	13 L/min	13 L/min
Auxiliary gas	0.8 L/min	0.8 L/min
Make up gas	~1 L/min	~1 L/min
Monitored masses (dwell times listed for *Agilent*)	^{238}U, ^{232}Th, ^{208}Pb, ^{207}Pb, ^{206}Pb, ^{204}Pb/^{204}Hg, ^{202}Hg	^{238}U(0.06), ^{207}Pb (0.13), ^{206}Pb (0.1), ^{204}Pb/^{204}Hg (0.1)
^{238}U sensitivity, dry solution	0.5% (23 Mcps/ppb)	0.1% (4 Mcps/ppb)

	Laser-Ablation System
Instrument model	Photon Machines Analyte 193
Laser	ATLEX-SI 193nm ArF excimer
Fluence	~1 J/cm^2
Repetition rate	10 Hz
Excavation rate	~0.07 um/pulse
Spot size	65–110 μm
Delay between analyses	20 s
Ablation duration	15 s
Carrier gas (He) flow (cell; cup)	0.12; 0.06 L/min

Table 2. Results from 3 experiments

sample #	C258	C273C	C304A	C283A	C283C	C254A
Experiment F (P3D - 238 on Faraday; 65 μm, ~2.7 mV/ppm U)						
total spots	110	100	100	100	100	100
$^{238}U/^{206}Pb$ 2σ <50%	54%	76%	63%	29%	38%	63%
spots for isochron	35%	76%	47%	21%	25%	n/a
average U ppb	40	195	286	28	25	456
median U ppb	30	73	96	25	27	55
average cps 238	7100	33800	46800	4600	4100	73100
median cps 238	5300	12700	15700	4100	4400	8800
avg. $^{238}U/^{206}Pb$ 2σ	28%	17%	17%	32%	35%	24%
maximum U/Pb_c	49	145	54	27	17	n/a
Age (Ma)	437 ± 18	80.9 ± 1.5	111.1 ± 2.1	453 ± 40	492 ± 81	n/a
final 2σ	4.1%	1.9%	1.9%	8.8%	16.5%	n/a
Experiment D (P3D - 238 on Daly; 65 μm, ~2.1–2.7 mV/ppm U)						
total spots	100	100	100	100	100	100
$^{238}U/^{206}Pb$ 2σ <50%	96%	98%	97%	97%	93%	90%
spots for isochron	75%	90%	84%	64%	68%	n/a
average U ppb	24	144	196	11	18	232
median U ppb	13	59	40	8	18	33
average cps 238	3800	24500	27900	1600	2400	29300
median cps 238	2100	10000	5700	1200	2400	4200
avg. $^{238}U/^{206}Pb$ (2σ)	16%	10%	12%	17%	16%	19%
maximum U/Pb_c	30	205	79	26	12	n/a
Age (Ma)	445 ± 11	83.5 ± 1.6	119.3 ± 2.3	430 ± 11	430 ± 14	n/a
final 2σ	2.5%	1.9%	1.9%	2.6%	3.3%	n/a
Experiment Q (Agilent 7700 Q-ICPMS; 110 μm, ~1.8 mV/ppm U)						
total spots	110	100	100			
$^{238}U/^{206}Pb$ 2σ <50%	96%	87%	94%			
spots for isochron	75%	87%	94%			
average U ppb	28	126	371			
median U ppb	14	68	80			
average cps 238	3100	14400	39400			
median cps 238	1600	7800	8500			
avg. $^{238}U/^{206}Pb$ (2σ)	20%	14%	13%			
maximum U/Pb_c	26	325	93			
Age (Ma)	460 ± 18	85.4 ± 2.0	118.1 ± 4.0			
final 2σ	3.9%	2.3%	3.4%			